



# The influence of liver fat deposition on the quantification of the liver-iron fraction using fast-kilovolt-peak switching dual-energy CT imaging and material decomposition technique: an *in vitro* experimental study

Tingting Xie<sup>1</sup>, Yongbin Li<sup>2</sup>, Guanyong He<sup>1</sup>, Zhen Zhang<sup>1</sup>, Qiao Shi<sup>1</sup>, Guanxun Cheng<sup>1</sup>

<sup>1</sup>Medical Imaging Center, <sup>2</sup>Department of Ultrasound Imaging, Peking University Shenzhen Hospital, Shenzhen 518036, China

Correspondence to: Guanxun Cheng. Medical Imaging Center, Peking University Shenzhen Hospital, Shenzhen 518036, China.

Email: Chengguanxun@hotmail.com.

**Background:** To assess the feasibility of dual-energy spectral computed tomography (DECT) for quantifying the liver iron content (LIC) with material decomposition (MD) technique *in vitro*.

**Methods:** Liver-iron mixture samples (model A) and liver-iron-fat mixture samples (model B) were prepared and scanned by a single source DECT using GSI mode with successive tube currents of 200, 320, and 485 mA. A standard algorithm of 1.25 mm was used to reconstruct iron (fat) MD images and iron (water) MD images. The iron concentrations of all samples were measured and analyzed by Spearman's rank correlation and linear regression analysis.

**Results:** Significant positive linear correlations were found between virtual iron content (VIC) and LIC in the absence of fat (model A) and in the presence of fat (model B) in the range of LIC 0 to 25 mg/mL. The lines of best fit to model A had slopes around 1.1 and an intercept around (-1.5) mg/mL for iron (water) MD images, and had slopes around 1.1 and an intercept around (-10) mg/mL for iron (fat) MD images. The lines of best fit to the model B had slopes around 1.5 and an intercept around (-15) mg/mL. At the same value of LIC (LIC >0), the VIC values of model A were always higher than those of model B. At the high value of LIC (12.5 mg/mL), the VIC values of model B were similar, but they differed greatly from those of model A.

**Conclusions:** The fast-kilovolt-peak switching dual-energy CT imaging and MD techniques allow for quantification of iron content. Fat and the post-reconstruction algorithm of iron (fat) MD images, were confounding factors, and led to the underestimation and overestimation of LIC, respectively.

**Keywords:** Single-source dual-energy CT; material decomposition (MD); liver; iron; fat

Submitted Oct 10, 2018. Accepted for publication Apr 09, 2019.

doi: 10.21037/qims.2019.04.06

View this article at: <http://dx.doi.org/10.21037/qims.2019.04.06>

## Introduction

Hepatic iron overload usually occurs in patients with hereditary hemochromatosis, which often results in an increase of CT values in liver parenchyma (1). The presence of iron overload is diagnosed when the CT value of the liver is greater than 75 HU on non-contrast enhanced CT (2). However, the increase of CT value cannot fully reflect the existence and severity of hepatic iron deposition,

which might be susceptible to fatty degeneration, glycogen deposition, anemia, and other factors. As a result, the degree of liver iron overload has been underestimated (3,4). The material decomposition (MD) technique in dual-energy spectral (DESCT) is one of the noninvasive imaging methods to evaluate iron overload in the liver. Severity of iron overload and the diagnosis of iron overload in patients with long-term blood transfusions can be assessed to guide the treatment of iron removal and evaluate the treatment

effect (5,6).

A few researchers have indicated that fat could be a compounding factor in the estimation of hepatic iron, and that the fat confounding effect could be eliminated by dual-energy CT. However, the results of these researchers were determined by an iron-specific three-MD algorithm, and a difference of averaged attenuation between 80 and 140 kVp at CT ( $\Delta H$ ) on dual-source dual-energy CT; in addition, the liver iron content (LIC) that was covered ranged from 0 to 6 mg/mL only (6-8). Using fast-kilovolt-peak switching dual-energy CT imaging and MD technique to study the liver iron quantification in the case of coexisting fat is rarely reported and the feasibility and accuracy is unknown; meanwhile, whether dual-energy CT is feasible for LIC above 6 mg/mL also remains unclear.

The purpose of our study was to assess the feasibility of the fast-kilovolt-peak switching dual-energy CT imaging and MD technique to evaluate the LIC from 0 to 25 mg/mL, even in the case of coexisting fat.

## Methods

### *Rat liver phantom*

This study was approved by the Research Animal Resource Center of Peking University Shenzhen Hospital. Twenty normal rats were dissected and the livers were isolated, washed, and shredded into homogenized solution to mix with different concentrations of dextriferron in polyvinylchlorid (PVC) tubes (volume: 4 mL; inner-diameter: 10 mm). Liver-iron mixture sample (model A) and liver-iron-fat mixture samples (model B) were prepared as follows: for model A (n=6), six homogeneous liver-iron samples were mixed with dextriferron to make the final iron concentration of 0.00, 1.56, 3.13, 6.25, 12.50, and 25.00 mg/mL; for model B, a total of 24 samples of 3 groups of homogeneous liver-iron mixed samples with iron concentration gradient of 0.00, 2.50, 5.00, 7.50, 10.00, and 12.50 mg/mL were prepared (group A, B, and C). Group A, B, and C had fat added with volume percentages of 2.5%, 7.5% and 15%, respectively (*Table 1*). To make the sample have a uniform appearance, the model was fully oscillated by the suspension oscillator (Misonix, Sonicator 4000, USA).

### *CT acquisition and image analysis*

The cylindrical phantoms used had a diameter of 20 cm,

with 9 tubes inside; the diameter of each tube was 25 mm, and the height was 97.6 mm. Each tube in the phantom was filled with a PVC tube, and then the phantom was scanned by using fast-kilovolt-peak switching dual-energy CT (80 and 140 kVp) with a 256-section multi-detector CT scanner (Revolution CT, GE healthcare, USA).

The scanning parameters were as follows: CT was used to scan the phantom 3 times, with the tube current of each scan being 200, 320, and 485 mA respectively; gantry rotation speed was 0.5 r/s; field of view display was 250 mm; reconstruction layer thickness was 1.25 mm; pitch was 0.984 mm; the reconstruction function was STND, and adaptive statistical iterative reconstruction-V (ASiR-V) was 50%.

All raw data were sent to the ADW 4.6 workstation and post-processing analysis was performed using GSI general MD analysis software to reconstruct the iron (fat) MD images and iron (water) MD images. By drawing one ROI on the upper, middle, and lower parts of each tube with a diameter of 6 mm and an area of 28.26 mm<sup>2</sup>, the mean value the three ROIs was recorded as the virtual iron content (VIC). VIC values were included in the database.

### *Statistical analysis*

Statistical software (SPSS 21.0) was used for statistical analysis. One-way analysis of variance (ANOVA) was performed on the corresponding VIC under the tube currents of 200, 320, and 485 mA to compare the effect of tube currents on the results of VIC. A P value less than 0.05 was considered to indicate statistical significance. The correlations between the VIC and LIC of group A, B, and C were evaluated by Spearman analysis. The regression lines for model A and B were assessed by analysis of covariance to determine if the liver fat deposition had statistically significant effects on VIC.

## Results

### *Results of model A*

The model A showed good linear relationship between the VIC and LIC; the fitted linear correlation equations are shown *Table 2*. There was no statistical difference in VIC between different mAs (P=0.993, F=0.007). The fitted linear correlation equations had similar slopes and different intercepts between iron (water) MD images and iron (fat) MD images. The intercepts of the fitted linear correlation

**Table 1** Material composition of the PVC tubes

PVC tube No.	Total volume (mL)	Preparation					
		Rat liver (mL)	Fat (mL)	Iron (mg)	Water (mL)	LFC (%)	LIC (mg/mL)
1	4.0	2.0	0	0	2.0	0	0
2	4.0	2.0	0	6.25	1.875	0	1.56
3	4.0	2.0	0	12.5	1.75	0	3.125
4	4.0	2.0	0	25	1.5	0	6.25
5	4.0	2.0	0	50	1	0	12.5
6	4.0	2.0	0	100	0	0	25.0
7	4.0	2.9	0.1	0	1	2.5	0
8	4.0	2.9	0.1	10	0.8	2.5	2.5
9	4.0	2.9	0.1	20	0.6	2.5	5.0
10	4.0	2.9	0.1	30	0.4	2.5	7.5
11	4.0	2.9	0.1	40	0.2	2.5	10.0
12	4.0	2.9	0.1	50	0	2.5	12.5
13	4.0	2.7	0.3	0	1	7.5	0
14	4.0	2.7	0.3	10	0.8	7.5	2.5
15	4.0	2.7	0.3	20	0.6	7.5	5.0
16	4.0	2.7	0.3	30	0.4	7.5	7.5
17	4.0	2.7	0.3	40	0.2	7.5	10.0
18	4.0	2.7	0.3	50	0	7.5	12.5
19	4.0	2.4	0.6	0	1	15	0
20	4.0	2.4	0.6	10	0.8	15	2.5
21	4.0	2.4	0.6	20	0.6	15	5.0
22	4.0	2.4	0.6	30	0.4	15	7.5
23	4.0	2.4	0.6	40	0.2	15	10.0
24	4.0	2.4	0.6	50	0	15	12.5

PVC, polyvinylchlorid.

equations on iron (fat) MD images were much higher than the slope of equation on iron (fat) MD images.

### Results of model B

Spearman analysis showed that VIC and LIC were highly positively correlated for groups A, B, and C, while the linear equations among the three groups were different (Table 2). The VIC values of model A were always greater than those of model B when the LIC was at the same value (Figure 1). This suggests that the presence of fat affects the

measurement of VIC. The presence of fat caused VIC to underestimate the concentration of liver iron.

### Discussion

Hepatic iron and fatty deposition often exist simultaneously in patients with idiopathic liver hemosiderosis and chronic liver disease, such as viral hepatitis, alcoholic fatty liver, and nonalcoholic fatty liver disease (9-11). The quantification of iron is important for the treatment of iron removal and to evaluate the treatment effect (12). We designed an *in vitro*

**Table 2** Correlation between LIC and VIC in the model of liver-iron-fat under different tube currents ( $\bar{x}\pm s$ )

Concentrations of fat (%)	Tube currents (mA)	Samples	Spearman analysis		Linear correlation equation	Adjusted R <sup>2</sup> value	P value	F value
			Correlation coefficient	P value				
0 (Iron-water)	200	6	1.000	0.000	$y=1.076x-1.602$	0.995	0	994.169
	320	6	1.000	0.000	$y=1.104x-1.193$	0.995	0	969.015
	284	6	1.000	0.000	$y=1.089x-1.461$	0.996	0	1,112.086
0 (Iron-fat)	200	6	1.000	0.000	$y=1.083x-10.756$	0.993	0.000	662.910
	320	6	1.000	0.000	$y=1.095x-10.074$	0.993	0.000	750.433
	485	6	1.000	0.000	$y=1.100x-10.621$	0.993	0.000	733.509
2.5	200	6	1.000	0.000	$y=1.823x-15.546$	0.972	0.000	176.750
	320	6	1.000	0.000	$y=1.924x-15.869$	0.962	0.000	126.074
	485	6	1.000	0.000	$y=1.894x-16.093$	0.950	0.001	96.823
7.5	200	6	1.000	0.000	$y=1.582x-12.708$	0.950	0.001	96.823
	320	6	1.000	0.000	$y=1.661x-12.643$	0.968	0.000	152.418
	485	6	1.000	0.000	$y=1.721x-13.440$	0.960	0.000	120.547
15	200	5	1.000	0.037	$y=1.189x-7.078$	0.813	0.036	27.489
	320	5	1.000	0.000	$y=1.603x-10.238$	0.936	0.005	59.715
	485	5	1.000	0.000	$y=1.488x-9.613$	0.910	0.008	41.455

LIC, liver iron content; VIC, virtual iron content.

experimental study to quantify the LIC using fast-kilovolt-peak switching dual-energy CT imaging and MD technique. The concentration of iron (0–25 mg/mL Fe) in the test tubes simulates the iron concentration in liver from healthy patients to that observed in pathologic states, including in patients with hereditary hemochromatosis and severe iron overload (>350 mg per 100 g liver wet weight) resulting in clinically relevant liver damage (13). Additionally, the concentration of fat (with 2.5%, 7.5% and, 15% volume percentage of fat simulating human mild and moderate fatty liver) in the test tubes varied from that observed in healthy patients to moderate fatty liver. The results of our study show that VIC was significantly correlated with the iron concentration of the liver-iron mixture samples, while VIC underestimated the value of LIC in the presence of fat, and the VIC value measured on the Iron (fat) MD images overestimated the value of LIC in the absence of fat.

Our study was not the only one to quantify LIC in the presence of fat by using dual-energy CT; recent studies have used different technologies to investigate the feasibility and accuracy of dual-energy CT in liver iron quantification.

Fischer *et al.* quantified LIC with coexisting fat and also quantified liver fat in the presence of iron and iodine in their *ex vivo* study with DECT, but the LIC covered in these studies ranged from 0 to 6 mg/mL only (6). Joe assessed the hepatic iron in liver phantoms and liver transplant recipients by calculating the CT attenuation (HU) difference between high and low tube voltages with DECT (5). Ma *et al.* separated the hepatic iron and fat when they coexisted by dual energy MD *in vivo* with DECT (7). These studies were all conducted with dual-source DECT, and the fat confounding effect in the estimation of hepatic iron was concluded to be eliminated. While few people have studied liver iron quantification by using fast-kilovolt-peak switching dual-energy CT, fast-kilovolt-peak switching dual-energy CT has been widely used in clinical work. Tomoko *et al.* assessed the ability of fast-kilovolt-peak switching dual-energy CT by using the multi-MD (MMD) algorithm to quantify liver fat *in vivo*, and found dual-energy CT fat volume fraction (FVF) led to underestimation of the liver fat contained in the presence of iron (14). The study, however, did not discuss the

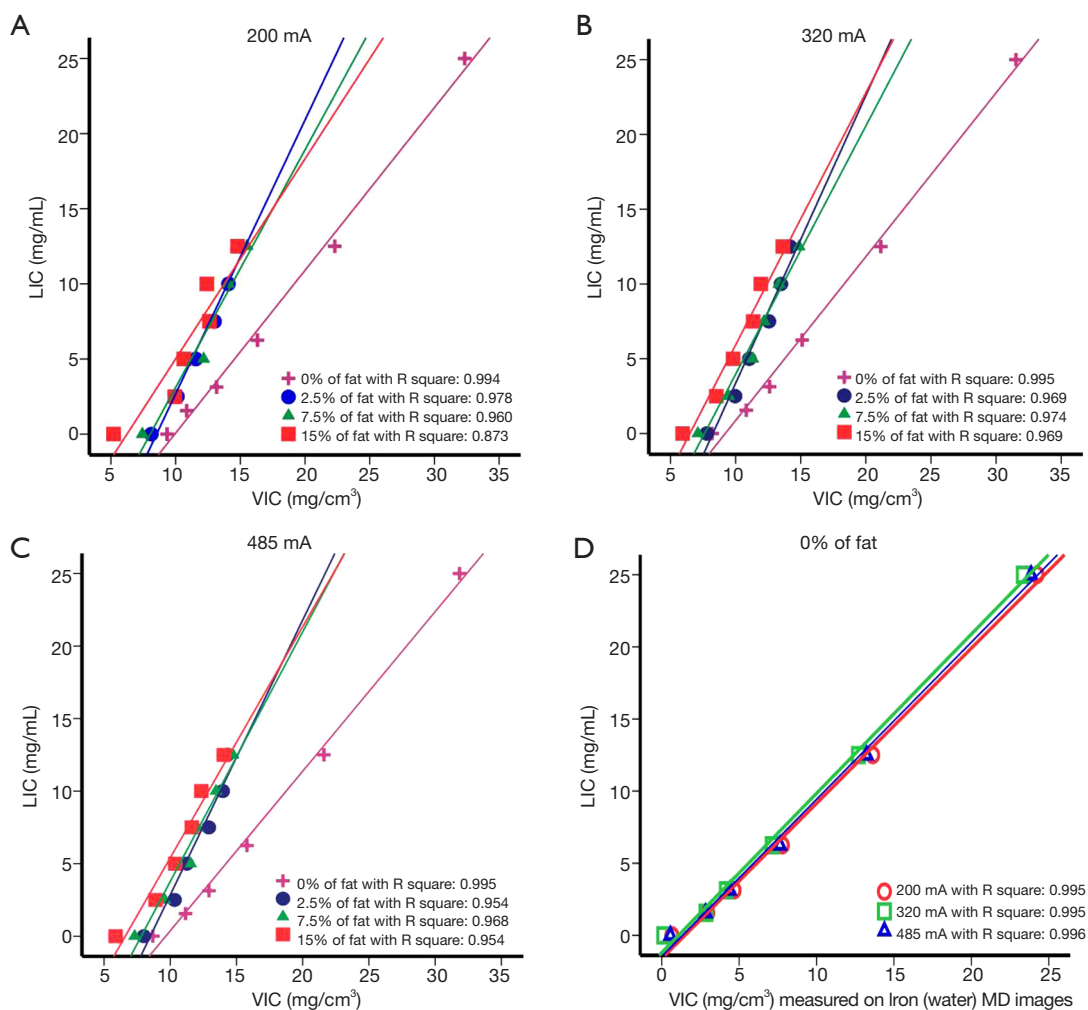


**Figure 1** Scatterplots of liver iron content (LIC) and virtual iron content (VIC) measured by using single source dual-energy CT on iron (fat) MD images for liver-iron phantoms with and without fat at tube currents of 200 (A), 320 (B), and 485 mA (C). The pink, blue, green, and red lines represent the regression lines for the 0%, 2.5%, 7.5%, and 15% of fat samples, respectively. (D) Scatterplots of LIC and VIC measured by using single source dual-energy CT on iron (water) MD images for the fat-free phantom. Spearman correlation coefficients are shown ( $P < 0.05$ ).

quantification of liver iron in the presence of fat.

First, our study verified that the fast-kilovolt-peak switching dual-energy CT imaging and MD technique can be used to quantify the liver iron concentration in fat-free phantom. The fat-free phantom showed a good linear relationship between the VIC and LIC (correlation coefficient, 1.00 and  $P < 0.001$ ), and the slopes of fitted linear correlation equations were 1.076, 1.104, and 1.089 at different tube currents which were quite similar to 1.0. The intercepts were  $-1.602$ ,  $-1.193$ , and  $-1.461$  on iron (water) MD images. The negative intercepts might be due

to the fact that homogeneous rat liver (2 mL) was contained in tube No. 1, and liver is rich in iron, which, due to the presence of a large number of hepatic sinusoids, resulted in a VIC value of more than 0 when the LIC was equal to 0. On Iron (fat) MD images, the fat-free phantom also showed good linear relationship between the VIC and LIC (correlation coefficient, 1.00 and  $P < 0.001$ ), and the slopes of fitted linear correlation equations were quite similar to 1.0, while the intercepts were around  $-10$ , which indicates that VIC values measured on the iron (fat) MD images overestimated the value of LIC in the fat-free phantom.

The fat-contained phantom also showed a good linear relationship between the VIC and LIC (correlation coefficient, 1.00 and  $P < 0.05$ ), while the slopes of fitted linear correlation equations varied from 1.5 to 1.9, which were quite different from 1.0. Furthermore, as seen in *Figure 1*, at the LIC value of 12.5 mg/mL, the VIC values of fat-contained phantom were similar, but quite different from the VIC values of fat-free phantom. From *Figure 1*, we found that for the same LIC (LIC > 0 mg/mL), the VIC values of the fat-free phantom were always higher than the VIC values of the fat-contained phantom on the tube current of 200, 320, and 485 mA, which indicates that the presence of fat caused VIC to underestimate LIC even when the volume percentage of fat was as low as 2.5%. We also noticed that the effect of fat causing VIC to underestimate the LIC value increased when the iron concentration decreased, as the difference between VIC values were 2.92 mg/cm<sup>3</sup> when the LIC was 0 mg/mL, and the differences were 1.23 mg/cm<sup>3</sup> when the LIC was 12.5 mg/mL. Therefore, we concluded that DECT imaging and MD technique might not be quite as accurate in the quantification of iron accumulation when the fat and iron coexist, especially for the lower levels of iron accumulation.

The effect of fat causing VIC to underestimate the LIC value being possibly similar to the negative DE index (i.e., negative  $\Delta H$ ; the difference of averaged attenuation between 80 and 140 kVp at CT was negative) of fat may have cancelled out the positive DE index  $\Delta H$  of iron, resulting in the underestimation of iron accumulation in DSDE CT (5).

The advantages of DECT for liver iron quantification over MRI are as follows: (I) DECT (0–25 mg/mL in our study) can determine higher iron concentration than MR (LIC  $\leq 30$  mg Fe/g in dry tissue, about LIC  $\leq 2.5$  mg/mL Fe in phantom study) (15); (II) the scanning speed of DECT is fast and the examination time is short, and usually it takes only one breath hold, which helps to decrease the artifacts caused by breathing movement and heart beat; (III) there is no need for additional scanning sequences or iodine contrast agents, and the estimation of iron in liver can be accomplished by unenhanced upper abdominal scan by GSI mode. No additional fee is required, and the cost of DECT is lower than that of MR examination.

It is well known that liver iron overload can also be assessed qualitatively by acquiring R2 mapping. However, the nonlinear relationship between R2 and LIC introduces complexity into the calibration, and the slow increase in R2 with LIC at high LIC values results in the reduced

precision of R2-based LIC measurements with severe iron overload. Furthermore, R2-based methods are known to be confounded by factors other than iron concentration, including the rate of diffusion (16), which limits the accuracy of R2-based quantification of LIC. The main limitation of R2-based liver iron quantification is the long acquisition time required for R2 mapping, particularly using SSE imaging sequences. In addition, these long acquisition times result in potentially severe motion artifacts in free-breathing acquisitions. These motion artifacts currently require careful manual delineation of ROIs in the St. Pierre method, complicating the workflow of iron quantification. R2\* mapping, based on gradient echo acquisitions, has the potential to overcome some of the limitations of R2-based techniques, due to its ability to provide full liver coverage without motion artifacts within a single breath-hold, whereas R2\* measurements will depend on the specific acquisition parameters. However, this is not a fundamental limitation of liver R2\* mapping as cases of extremely rapid signal decay may impose a limitation for accurate liver iron quantification in the presence of massive iron overload, even at 1.5 T (17).

MRI-based quantitative susceptibility mapping (QSM) techniques have been developed and validated over recent years (18–20), and from the liver susceptibility estimates, LIC can be assessed (21). However, QSM constitutes a challenging mathematical problem (22–24). QSM has primarily focused on applications in the brain, and abdominal QSM is less developed due to several additional challenges, including the presence of motion, fat, and multiple tissue/air interfaces. Recently, a QSM technique for the abdomen was developed, and its feasibility was demonstrated in patients with liver iron overload (25). This technique addresses the challenges of QSM outside of the brain, including the presence of fat, physiological motion during acquisition, as well as the potential for large susceptibility shifts, which increases R2\* signal decay.

Although appealing, susceptibility estimation techniques present several limitations for iron quantification, including uncertainty in converting susceptibility measurements to liver iron concentration values. This conversion may depend on the relative concentration of ferritin and hemosiderin, which in turn may depend on the type of iron overload and give rise to inter-organ, inter-patient, or inter-disease variability (25,26). Currently, the main drawback of susceptibility mapping techniques compared to relaxometry is likely the complication of the estimation problem. Although sophisticated QSM techniques have

been proposed in recent years, significant development and validation are needed before QSM-based liver iron quantification becomes clinically applicable.

Because the MD technique is model-based and uses National Institute-of-Standards-and-Technology-measured values (27) to obtain the linear attenuation space (16), the MD technique itself is generalizable.

This study had several limitations. First, the slopes of the fitted linear correlation equations were not exactly equal to 1.0, and the X-axis intercepts were -1.602, -1.193, and -1.461, but not 0. It might have been caused by the following reasons. (I) The mixtures of homogenous rat liver and iron looked uniform by eye and there was no stratification. In fact, the liver and the iron Dextran-complex in each ROI might not have been mixed perfectly and uniformly, and we only drew three ROIs in each tube which led to the three VIC values not being fully reflected in the LIC of each tube. If we drew more ROIs in each tube, the slope might have been closer to 1.0; (II) there may be stratification of samples that could not be recognized by the eyes although the samples looked uniform. We drew one ROI on the upper, middle, and lower parts of each tube, and the unrecognizable stratification made VIC values on the upper part of the tubes underestimate the LIC; (III) the homogenous rat liver was viscous and easily adhered to the wall of the pipette; it could not be completely removed into the PVC tube, so the real volume of rat liver in each tube was not exactly the same as that calculated in *Table 1*.

In conclusion, the fast-kilovolt-peak switching dual-energy CT imaging and MD technique allows for quantification of iron content. The presence of fat and the post-reconstruction algorithm of iron (fat) MD images, were confounding factors, leading to the underestimation and overestimation of LIC, respectively.

### Acknowledgements

Special thanks to Ying Guo and Jin Guo from GE Healthcare (China) CT Research Center for their selfless technical guidance.

### Footnote

*Conflicts of Interest:* The authors have no conflicts of interest to declare.

*Ethical Statement:* This study was approved by the Research Animal Resource Center of Peking University Shenzhen

Hospital (No. SYXK2015-0106).

### References

1. Deugnier Y, Turlin B. Pathology of hepatic iron overload. *Semin Liver Dis* 2011;31:260-71.
2. Sanyal AJ. American Gastroenterological Association. AGA technical review on nonalcoholic fatty liver disease. *Gastroenterology* 2002;123:1705-25.
3. Qayyum A. MR spectroscopy of the liver: principles and clinical applications. *RadioGraphics* 2009;29:1653-64.
4. Luo XF, Xie XQ, Cheng S, et al. Dual-Energy CT for Patients Suspected of Having Liver Iron Overload: Can Virtual Iron Content Imaging Accurately Quantify Liver Iron Content? *Radiology* 2015;277:95-103.
5. Joe E, Kim SH, Lee KB et al. Feasibility and accuracy of dual-source dualenergy CT for noninvasive determination of hepatic iron accumulation. *Radiology* 2012;262:126-35.
6. Fischer MA, Gnannt R, Raptis D, et al. Quantification of liver fat in the presence of iron and iodine: an ex-vivo dual-energy CT study. *Invest Radiol* 2011;46:351-8.
7. Ma J, Song ZQ, Yan FH. Separation of hepatic iron and fat by dual-source dualenergy computed tomography based on material decomposition: an animal study. *PLoS One* 2014;9:e110964.
8. Fischer MA, Reiner CS, Raptis D, et al. Quantification of liver iron content with CT-added value of dual-energy. *Eur Radiol* 2011;21:1727-32.
9. Aigner E, Theurl I, Theurl M, et al. Pathways underlying iron accumulation in human nonalcoholic fatty liver disease. *Am J Clin Nutr* 2008;87:1374-83.
10. Silva M, Silva ME, de Paula H, et al. Iron overload alters glucose homeostasis, causes liver steatosis, and increases serum triacylglycerols in rats. *Nutr Res* 2008;28:391-8.
11. Sebastiani G, Walker AP. HFE genein primary and secondary hepatic iron overload. *World J Gastroenterol* 2007;13:4673-89.
12. Paisant A, d'Assignies G, Bannier E, et al. MRI for the measurement of liver iron content, and for the diagnosis and follow-up of iron overload disorders. *Presse Med* 2017;46:e279-87.
13. Nielsen P, Engelhardt R, Düllmann J, et al. Non-invasive liver iron quantification by SQUID-biosusceptometry and serum ferritin iron as new diagnostic parameters in hereditary hemochromatosis. *Blood Cells Mol Dis* 2002;29:451-8.
14. Tomoko Hyodo, Masatoshi Hori, Peter Lamb. Multimatierial Decomposition algorithm for the

- Quantification of liver Fat content by Using Fast-Kilovolt-Peak switching Dual-energy CT: Experimental Validation. *Radiology* 2017;282:381-9.
15. Hernando D, Levin YS, Sirlin CB, et al. Quantification of liver iron with MRI: state of the art and remaining challenges. *J Magn Reson Imaging* 2014;40:1003-21.
  16. Ghugre NR, Wood JC. Relaxivity-iron calibration in hepatic iron overload: probing underlying biophysical mechanisms using a Monte Carlo model. *Magn Reson Med* 2011;65:837-47.
  17. Meloni A, Positano V, Keilberg P, et al. Feasibility, reproducibility, and reliability for the T\*2 iron evaluation at 3 T in comparison with 1.5 T. *Magn Reson Med* 2012;68:543-51.
  18. Haacke EM, Liu S, Buch S, et al. Quantitative susceptibility mapping: current status and future directions. *Magn Reson Imaging* 2015;33:1-25.
  19. Wang Y, Liu T. Quantitative susceptibility mapping (QSM): Decoding MRI data for a tissue magnetic biomarker. *Magn Reson Med* 2015;73:82-101.
  20. Liu C, Li W, Tong KA, et al. Susceptibility-weighted imaging and quantitative susceptibility mapping in the brain. *J Magn Reson Imaging* 2015;42:23-41.
  21. Schenck JF. The role of magnetic susceptibility in magnetic resonance imaging: MRI magnetic compatibility of the first and second kinds. *Med Phys* 1996;23:815-50.
  22. de Rochefort L, Liu T, Kressler B, et al. Quantitative susceptibility map reconstruction from MR phase data using bayesian regularization: validation and application to brain imaging. *Magn Reson Med* 2010;63:194-206.
  23. de Rochefort L, Brown R, Prince MR, et al. Quantitative MR susceptibility mapping using piece-wise constant regularized inversion of the magnetic field. *Magn Reson Med* 2008;60:1003-9.
  24. Liu J, Liu T, de Rochefort L, et al. Morphology enabled dipole inversion for quantitative susceptibility mapping using structural consistency between the magnitude image and the susceptibility map. *Neuroimage* 2012;59:2560-8.
  25. Hernando D, Cook RJ, Diamond C, et al. Magnetic susceptibility as a B0 field strength independent MRI biomarker of liver iron overload. *Magn Reson Med* 2013;70:648-56.
  26. Hackett S, Chua-anusorn W, Pootrakul P, et al. The magnetic susceptibilities of iron deposits in thalassaemic spleen tissue. *Biochim Biophys Acta* 2007;1772:330-7.
  27. Mendonca PR, Lamb P, Sahani DV. A flexible method for multi-material decomposition of dual-energy CT images. *IEEE Trans Med Imaging* 2014;33:99-116.

**Cite this article as:** Xie T, Li Y, He G, Zhang Z, Shi Q, Cheng G. The influence of liver fat deposition on the quantification of the liver-iron fraction using fast-kilovolt-peak switching dual-energy CT imaging and material decomposition technique: an *in vitro* experimental study. *Quant Imaging Med Surg* 2019;9(4):654-661. doi: 10.21037/qims.2019.04.06